TU Delft

Delft University of Technology

Bio-inspired combinable self-powered soft device operating during the disintegration and reconstruction for next-generation artificial electric organs

Chen, Yuanyuan; Dai, Hanqing; Hu, Zhe; Wei, Jinxin; Zhou, Wenjie; Duan, Zhongtao; Cui, Zhongjie; Wei, Wei; Zhang, Guoqi; More Authors

DOI
10.1016/j.apmt.2023.101836

Publication date
2023

Document Version
Final published version

Published in
Applied Materials Today

Citation (APA)
Chen, Y., Dai, H., Hu, Z., Wei, J., Zhou, W., Duan, Z., Cui, Z., Wei, W., Zhang, G., & More Authors (2023). Bio-inspired combinable self-powered soft device operating during the disintegration and reconstruction for next-generation artificial electric organs. *Applied Materials Today*, *32*, Article 101836. https://doi.org/10.1016/j.apmt.2023.101836

Important note
To cite this publication, please use the final published version (if applicable).
Please check the document version above.

Copyright
Other than for strictly personal use, it is not permitted to download, forward or distribute the text or part of it, without the consent of the author(s) and/or copyright holder(s), unless the work is under an open content license such as Creative Commons.

Takedown policy
Please contact us and provide details if you believe this document breaches copyrights.
We will remove access to the work immediately and investigate your claim.

This work is downloaded from Delft University of Technology.
For technical reasons the number of authors shown on this cover page is limited to a maximum of 10.

Green Open Access added to TU Delft Institutional Repository

'You share, we take care!' - Taverne project

https://www.openaccess.nl/en/you-share-we-take-care

Otherwise as indicated in the copyright section: the publisher is the copyright holder of this work and the author uses the Dutch legislation to make this work public.

Applied Materials Today 32 (2023) 101836

Contents lists available at ScienceDirect

Applied Materials Today

journal homepage: www.elsevier.com/locate/apmt

Bio-inspired combinable self-powered soft device operating during the disintegration and reconstruction for next-generation artificial electric organs

Yuanyuan Chen [a], Hanqing Dai [b,*], Zhe Hu [a], Jinxin Wei [a], Wenjie Zhou [a], Zhongtao Duan [a], Zhongjie Cui [a], Wei Wei [d,*], Guoqi Zhang [c,*], Wanlu Zhang [a,*], Ruiqian Guo [a,*]

[a] Institute for Electric Light Sources, School of Information Science and Technology, Fudan University, Shanghai 200433, China
[b] Academy for Engineering and Technology, Fudan University, Shanghai 200433, China
[c] Department of Microelectronics, Delft University of Technology, Delft 2628 CD, Netherlands
[d] College of Electronic and Optical Engineering, Nanjing University of Posts and Telecommunications, Nanjing 210023, China

ARTICLE INFO

Keywords:
Self-powered sensors
Hydrogel sensor array
Disintegration
Reconstruction
Combinable ability
Programmable intelligent identification model

ABSTRACT

Hydrogel materials have biocompatibility, flexibility, transparency, self-healing ability, adhesion with various substrates, anti-freeze ability, and high-temperature resistance. However, the existing hydrogel devices cannot continue to operate in the case of damage, and they cannot work during the repair period, which brings great challenges and threats to life safety. Herein, we have designed a bio-inspired combinable low-power device by imitating the generation of nerve signals whose components can be disassembled and can continue to operate during the period of reconstruction. And the mechanism and determinants of the above phenomena are revealed. The results indicate that this device can establish some information interaction relationships with the body or its surroundings to reflect and identify certain changes, implying that it will possess promising potential in feedback systems, power transformers, intelligence systems, soft robotics, wearable devices, implanted electronics with flexible characteristics matching biological tissues, etc.

1. Introduction

Recently, with the development of artificial intelligence systems, soft robotics and wearable devices, implanted electronics with flexible characteristics matching biological tissues have increasingly attracted attention [1–8], especially in the low-power implanted electronics, such as retina implants, cochlear implants, deep-brain stimulators and spinal-cord stimulators [9–12], because they can receive and transmit the biological electrical signals from the brain, heart and muscle. However, the reported low-power implanted electronics mostly depend on the current amplifier, array sensor and control circuit to sense the external stimuli along with a power supply to provide power. Unfortunately, they cannot continue to work once any of the electric components is damaged.

Since hydrogel materials are found exhibiting biocompatible, flexible, transparent [13,14], self-healing [15,16], adhesive to various substrates [17–19], anti-freezing, resistant to high temperature [19–22]. Thus, self-healing hydrogel devices have been proposed to remedy the defects of electronic components [23–25]. Nevertheless, these reported hydrogel devices cannot continue to operate without self-repair in case of damage [13–25], and these hydrogel devices need a long time to complete reconstruction. These disadvantages make them unable to work during this period of reconstruction and bring great challenges and threats to life safety.

As is well known, a gecko's broken tail can jump for a while because it contains many nerves. Inspired by this action, we have designed a flexible and combinable low-power device by imitating the generation of nerve signals, and the device components can be disassembled and can continue to operate during the period of reconstruction. Also, the mechanism and determinants of the above phenomena are revealed. These results indicate that it will bring new inspirations to feedback systems, power transformers, intelligence systems, soft robotics, wearable devices, implanted electronics with flexible characteristics matching biological tissues, etc.

* Corresponding authors.
E-mail addresses: 98dhq@sina.com (H. Dai), weiwei@njupt.edu.cn (W. Wei), G.Q.Zhang@tudelft.nl (G. Zhang), fdwlzhang@fudan.edu.cn (W. Zhang), rqguo@fudan.edu.cn (R. Guo).

https://doi.org/10.1016/j.apmt.2023.101836
Received 23 December 2022; Received in revised form 20 April 2023; Accepted 30 April 2023
Available online 18 May 2023
2352-9407/© 2023 Elsevier Ltd. All rights reserved.

2. Results and discussion

A source of inspiration for design is revealed in Fig. 1. When the gecko encounters an enemy attack, its muscles contract violently, causing its tail to fall off. The tail, which has just broken off, keeps moving because the nerves are not dead. And the broken tail can continue to produce nerve impulses which can stimulate the synaptic vesicle to release neurotransmitters into the synaptic cleft after reaching the presynaptic membrane. Then, the combination of neurotransmitter and postsynaptic membrane receptor protein can stimulate the change of membrane potential, thus forming a current that will change the permeability of the adjacent nerve membrane to generate action potentials. These behavior goes on repeatedly, which can make nerve impulses from one position to another and then produce neural electric signals to guide the broken tail to continue shaking. Inspired by this, we designed a flexible and combinable self-powered device composed of H-C-L-A-H (namely, high-salinity (H), cation-selective (C), low-salinity (L) and anion-selective (A) gels, prepared by free radical polymerization with mold method) array by imitating the generation of nerve signals (Fig. 1).

As displayed in Fig. 2a–d, the morphologies of gels were observed by scanning electron microscope (SEM). It could be seen that the surface of L gel adding a small amount of $ZnCl_2$ was smooth (Fig. 2a), while the surface of H gel containing a large amount of $ZnCl_2$ was uneven (Fig. 2b). Besides, C gel with sodium isethionate showed a distinct layered structure (Fig. 2c), and A gel with the addition of (3-acrylamidopropyl) trimethylammonium chloride displayed a distinct granular shape (Fig. 2d). Additionally, the FT-IR spectra of the L, H, C and A gels were revealed that a series of characteristic bands at 3315 (N-H), 1652 (C=O), 1454 (CH_2), 1415 (C-N), and 1125 (NH_2) cm^{-1} correspond to the polyacrylamide hydrogel (Fig. 2e) [26–29]. Moreover, the peaks at 1030 cm^{-1} in the C gel and 965 cm^{-1} in the A gel were attributed to $-SO_3^-$ stretching vibration from sodium isethionate and $-N^+(CH_3)_3$ stretching vibration from (3-acrylamidopropyl) trimethylammonium chloride, respectively. These two characteristic peaks which were visible indicated the successful introduction of the exchangeable cationic and anionic group into the polymer chain. However, the bands at 3315 cm^{-1} corresponding to N-H stretching were shifted to 3293 cm^{-1} in the H gel and the bands at 1125 cm^{-1} corresponding to the NH_2 in-plane rocking were shifted to 1105, 1093, and 1173 cm^{-1}, respectively, in the L, A and C gels [26–29]. Consequently, the shifts of the characteristic peaks fully implied that there were strong hydrogen-bonding interactions between the acylamino groups of polyacrylamide hydrogel chains and exchangeable cationic and anionic groups [26–29].

Furthermore, the flexible abilities of L, H, C and A gels were investigated (*Supporting Information Part 1*). The parameters of hardness were 12 (L gel), 14 (H gel), 19 (C gel) and 17 (A gel) HA respectively and the parameters of young modulus were 0.21 (L gel), 0.32 (H gel), 0.20 (C gel) and 0.23 (A gel) MPa respectively (Fig. S1). The elastic stiffness coefficients were 5130.0 (L gel), 7877.5 (H gel), 5037.5 (C gel) and 5542.5 (A gel) $N{\cdot}m^{-1}$ (Fig. S1), which means that the outer H gel layer would only produce small deformation when subjected to external forces and the secondary outer C gel layer could be served as an external pressure buffer area in the H-C-L-A-H device. Therefore, this structure possessed a brilliant advantage to protect the stability of the internal structure.

As illustrated in Fig. 3a, the current-time relationship implied that the initial current of the self-powered H-C-L-A-H device was approximately 19 μA. In 0–800 s, the output current dropped with time. Moreover, the initial voltage was about 141.27 mV, rapidly rising to the maximum value of 147.60 mV within 0–10.2 s, and then decreased. The maximum power was about 2.80 μW. As an exhaustive explanation, the mechanisms were revealed (Fig. 3b). Firstly, it is well known that ions diffuse from high concentration to low concentration in solution. Since the water contents of H, L, A and C gels were 176.05, 379.37, 147.46 and 167.83% respectively, the water of the L gel spread towards A and C gels respectively (Fig. 3b), and the ionization of $ZnCl_2$ near A and C gels was accelerated during this process. Due to a lot of (3-acrylamidopropyl) trimethylammonium chloride and sodium isethionate in A and C gels respectively, Zn^{2+} ions produced from ionization in L gel first spread to C gel, and Cl^- ions initially spread to A gel, thus the output voltage rapidly rose within 0–10.2 s while the output current dropped with time. And Zn^{2+} ions in the H gel contacting C gel spread to C gel. Initial Cl^- ions generated from ionization in the H gel contacting A gel spread to A gel. Moreover, with $ZnCl_2$ ionization in the H and L gels as well as the diffusion of Zn^{2+} and Cl^- ions, a chemical reaction occurred to form Zn $(OH)_2$ precipitation ($Zn^{2+} + 2OH^- \Leftrightarrow Zn(OH)_2\downarrow$) in the H, L, A and C gels. As the discharge time, Zn^{2+} and OH^- freedom ions gradually reduced in the H, L, A and C gels. Thus, when the chemical reaction of $Zn(OH)_2$ precipitation reached equilibrium ($c(Zn^{2+})=10^{-5}$ mol/L), the free conductive ions were mainly H^+ and Cl^- ions in the H, L, A and C gels, namely, these ions maintaining the H-C-L-A-H device were mainly H^+ and Cl^- ions. Therefore, both the voltage and current of the H-C-L-A-H device gradually declined with discharge time.

To profoundly understand the electrical ability of the H-C-L-A-H device, we regarded the migration of Zn^{2+}, H^+, Cl^- and OH^- ions as ideal interlayer diffusion based on the Donnan equilibrium theory, ignoring other factors such as water permeation, effects of functional groups, etc. And we introduced the ion diffusion equations to explain the mechanisms (detailed in *Supporting Information Part 2*).

Additionally, the effects of the number of cation-selective groups ($-SO_3^-$) (Fig. 3c–h) and anion-selective groups ($-N^+(CH_3)_3$) (detailed in *Supporting Information Part 3*) on the electrical properties were evaluated respectively. To evaluate the effect of the number of cation-selective

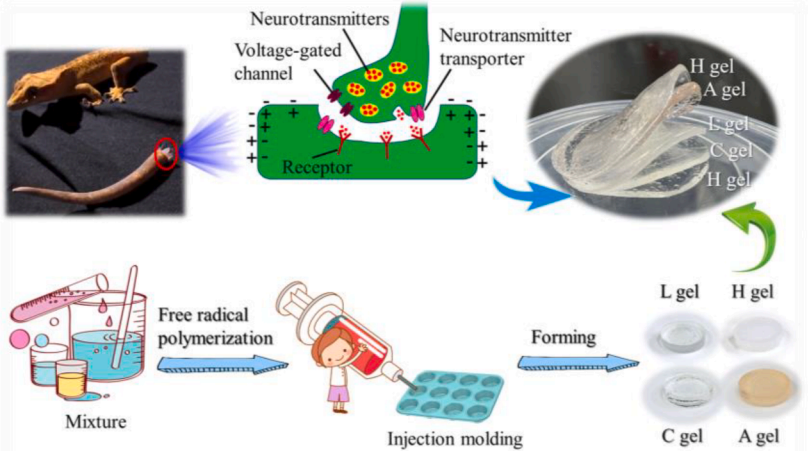

Fig. 1. The cartoon and photo of the design principle and materials synthesis of the flexible and combinable self-powered device. Here, $ZnCl_2$ electrolyte is used as a transport ion source, and Zn^{2+}, Cl^-, H^+ and OH^- ions are applied to simulate the neurotransmitter transmission. Besides, C and A gels played the role of voltage-gated ion channels. In addition, C gels allowed only cations to pass more easily, and correspondingly, A gels only permitted anions to go through more easily. Therefore, the H-C-L-A-H array could control ion exchanges to produce currents and voltages to obtain the self-powered ability.

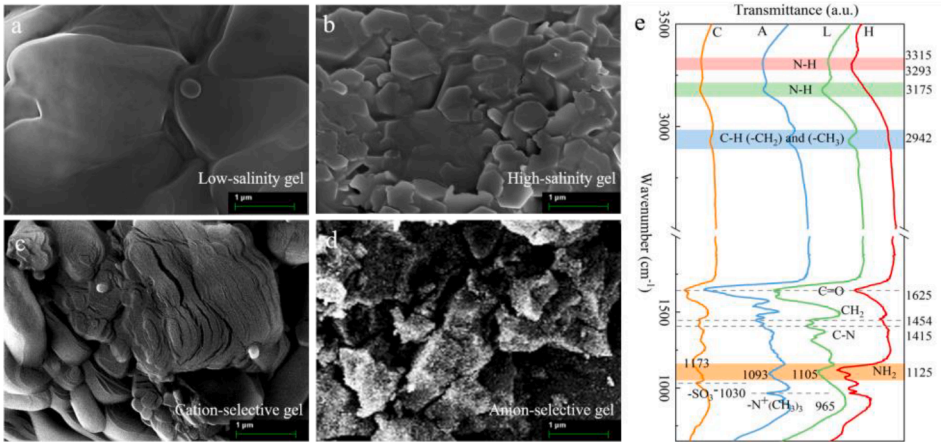

Fig. 2. The morphologies and structures of L, H, C and A gels. SEM images of dried L gel (a), H gel (b), C gel (c) and A gel (d). (e) FT-IR spectra of dried C, A, L and H gels.

groups ($-SO_3^-$) in C gel on the electrical properties of H-C-L-A-H overall structure, we prepared C gels containing 0.005, 0.01, 0.015, 0.02, 0.025 and 0.03 mol sodium isethionate (cation-selective groups: $-SO_3^-$), which were referred to as $C_{0.5}$, C_1, $C_{1.5}$, C_2, $C_{2.5}$ and C_3 gel, respectively. The electrical properties of these structures (H-$C_{0.5}$-L-A-H, H-C_1-L-A-H, H-$C_{1.5}$-L-A-H, H-C_2-L-A-H, H-$C_{2.5}$-L-A-H and H-C_3-L-A-H) were measured, respectively, as shown in Fig. 3c–h. The results indicated that the current-voltage-time relationships of H-$C_{1.5}$-L-A-H hydrogel components (Fig. 3e) were basically consistent with the H-C-L-A-H device (Fig. 3a). When the number of $-SO_3^-$ groups in C gel decreased, such as in $C_{0.5}$ and C_1 gels (Fig. 3c and d), the current and voltage decreased rapidly and then slowly. Besides, when the number of $-SO_3^-$ groups in C gel increased, such as in C_2, $C_{2.5}$ and C_3 gels (Fig. 3f–h), the current and voltage presented multiple complex change stages.

At first, the current-voltage-time relationships of the H-$C_{1.5}$-L-A-H device (Fig. 3e) were basically similar to that of the H-C-L-A-H device (Fig. 3a). The current decreased rapidly at first, then increased at 122.7 s, while the voltage increased slightly at the beginning and then decreased gradually at 18.3 s. Additionally, when the number of $-SO_3^-$ groups in C gel decreased, such as in $C_{0.5}$ and C_1 gels, the currents and voltages of H-$C_{0.5}$-L-A-H and H-C_1-L-A-H devices showed a rapid and then slow decline (Fig. 3c and d). Ions diffused rapidly under the concentration difference at the beginning, thus the current and voltage dropped rapidly. However, due to the fewer cation-selective groups ($-SO_3^-$) of $C_{0.5}$ and C_1 gels and the lack of binding sites for some cations, which made it difficult for cations to pass through, free ions of Zn^{2+} and OH^- gradually decreased with the formation and precipitation of Zn$(OH)_2$. Therefore, when the chemical reaction of Zn$(OH)_2$ precipitation reached equilibrium in H, L, A and C gels, the voltages and currents of H-$C_{0.5}$-L-A-H and H-C_1-L-A-H devices dwindled (Fig. 3c and d). However, when the number of $-SO_3^-$ groups in C gel increased, there were some differences. Generally speaking, the voltages and currents of H-C_2-L-A-H, H-$C_{2.5}$-L-A-H and H-C_3-L-A-H devices appeared to the multi-stages process of rising and falling (Fig. 3f–h). When the cation-selective groups ($-SO_3^-$) of C gel providing binding sites for cations increased, the initial migration speed of cations increased, which also affected the ionization of H_2O and $ZnCl_2$ and ions diffusion, therefore the current and voltage dropped rapidly at the beginning. The H^+ and Zn^{2+} ions near C_2, $C_{2.5}$ and C_3 gels had more opportunities to spread owing to the more cation-selective groups ($-SO_3^-$), causing the current to rise, in which case the anions accumulated on the left side in the H gel contacting C gel, thus the voltage gradually increasing (Fig. 3f–h). However, the number of anion-selective groups ($-N^+(CH_3)_3$) of A gel did not change, accordingly, some anions in L gel spread to H gel through A gel, resulting in a slight decrease in voltage. Then, with the formation and precipitation of Zn$(OH)_2$, more H^+ ions are generated in H gel contacting A gel, causing the voltage to climb. When the chemical reaction of Zn$(OH)_2$ reached equilibrium, the free conductive ions were mainly H^+ and Cl^- ions in the H, L, A and C gels, and therefore the voltages and currents of H-C_2-L-A-H, H-$C_{2.5}$-L-A-H and H-C_3-L-A-H devices gradually declined (Fig. 3f–h).

Furthermore, the results revealed that the rate of the current decline is affected by the water content and the number of cation-selective groups ($-SO_3^-$) of C gel. As illustrated in Fig. 3e–h, the rate of the current decline increased when the number of $-SO_3^-$ groups in C gel was below 0.015 mol (Fig. 3e) or reached 0.03 mol (Fig. 3h), while it entered a steady phase in the range of 0.015–0.025 mol (Fig. 3e–g). When the number of cation-selective groups ($-SO_3^-$) in C gel was small, the water content decreased with the increase of cation-selective groups ($-SO_3^-$), resulting in the decline of initial water diffusion to the ends of C gel. Accordingly, the initial formation and precipitation of Zn$(OH)_2$ declined, and therefore the rate of the current decline fell. However, the situation was a little different when the number of $-SO_3^-$ groups in C gel was 0.01 mol (Fig. 3d), where the current decline rate jumped due to more Zn^{2+} and H^+ ions generated that could spread and combine with $-SO_3^-$ groups faster. Moreover, when the number of cation-selective groups ($-SO_3^-$) in C gel was large, the action of the current became more complex according to the previous analysis, and the rate of the current decline entered a steady phase because of the number of cation-selective groups ($-SO_3^-$) and the water content. However, there were some differences when the number of $-SO_3^-$ groups in C gel was 0.03 mol (Fig. 3h), where the rate of the current decline surged because Zn^{2+} and H^+ ions both had the chance to combine with cation-selective groups ($-SO_3^-$) at this time due to the excessive number of $-SO_3^-$ groups in C gel compared with Zn^{2+} and H^+ions.

Similarly, the effect of the number of anion-selective groups ($-N^+(CH_3)_3$) in the A gel on the electrical properties of H-C-L-A-H overall structure was thoroughly investigated (detailed in *Supporting Information Part 3* and Fig. S2). In summary, all the results indicated that the A gel containing 0.012 mol (3-acrylamidopropyl) trimethylammonium chloride and the C gel containing 0.012 mol sodium isethionate became the ultimate selection due to the better electrical properties of the large initial current and voltage (19.389 μA and 141.27 mV) and the moderate current decline rate (3.31 μA/s).

To explore the combinable ability of the H-C-L-A-H device, the systemic combinable ability and the structural combinable ability were discussed respectively (Fig. 4). Firstly, the systemic combinable ability was revealed in Fig. 4a and *Supporting Video*. The H-C-L-A-H device was cut into two halves, as shown in the illustration of Fig. 4a, and a half could discharge in 11–53 s. After the two halves were reassembled into a whole, these could discharge in 90–139 s. Then, the upper half was removed, the rest worked in 161–204 s. After the two halves were reassembled into a whole, these still worked well in 265–321 s (Fig. 4a).

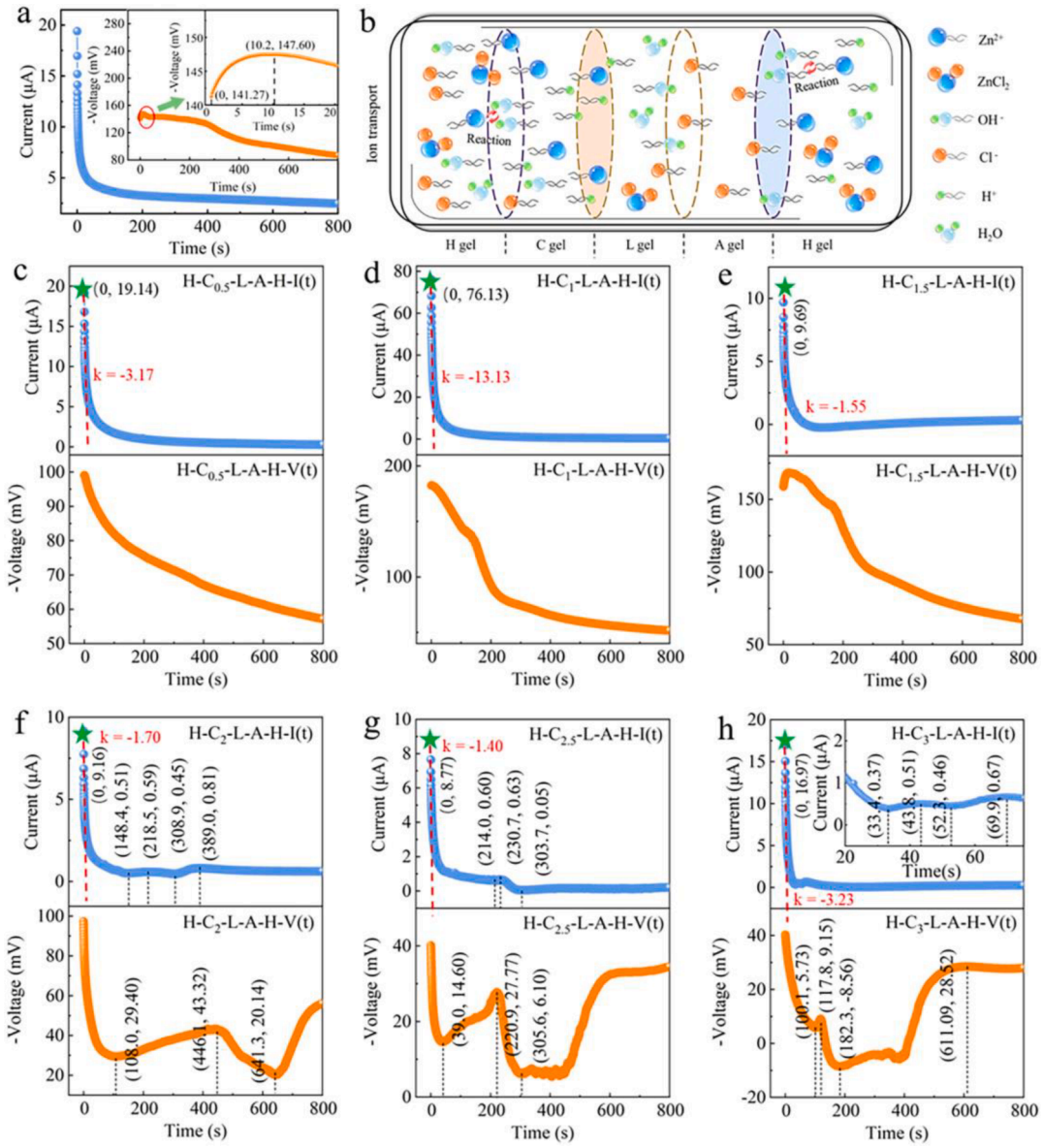

Fig. 3. Current-voltage-time relationships and ion transport mechanism. (a) Current-voltage-time relationships of H-C-L-A-H device. (b) Ion transport mechanism of -H-C-L-A-H device. The current-voltage-time relationships and the rates of the current decline of (c) -H-$C_{0.5}$-L-A-H, (d) -H-C_1-L-A-H, (e) -H-$C_{1.5}$-L-A-H, (f) -H-C_2-L-A-H, (g) -H-$C_{2.5}$-L-A-H and (h) -H-C_3-L-A-H devices. The C gels containing 0.005, 0.01, 0.015, 0.02, 0.025 and 0.03 mol sodium isethionate (cation-selective groups: -SO_3^-) were referred to as $C_{0.5}$, C_1, $C_{1.5}$, C_2, $C_{2.5}$ and C_3 gel, respectively. The minus (-) in front of the voltages in the ordinate titles represented the direction.

Thus, these results suggest that the H-C-L-A-H device has a superior systemic combinable ability that could discharge whether it is divided into two parts or reassembled into a whole.

Most importantly, the structural combinable ability was displayed in Fig. 4b–j. This characteristic can ensure that the H-C-L-A-H device can continue to operate in case of damage without self-repair, and the undamaged part can work during the reconstruction. Firstly, the outermost gel was removed, then the current-voltage-time relationships and ion transport of the remaining components (H-C-L-A and H-A-L-C) were explored in Fig. 4b and c. The currents of the H-C-L-A and H-A-L-C components first dropped rapidly and then stayed at a relatively weak value, while the voltages rose rapidly and then dropped. That was due to a chemical reaction forming $Zn(OH)_2$ precipitation ($Zn^{2+} + 2OH^- \Leftrightarrow Zn(OH)_2\downarrow$), where Zn^{2+} ions from $ZnCl_2$ ionization. In addition, C gels allowed only cations to pass more easily, and correspondingly, A gels only allowed anions to go through more easily. It is well known that ions diffuse from high concentration to low concentration in solution. Therefore, with the chemical reaction of $Zn(OH)_2$ precipitation and the free diffusion of ions in the H-C-L-A and H-A-L-C components, it would lead to the occurrence of these phenomena in currents and voltages.

Additionally, two gels of the H-C-L-A-H device were removed, then the current-voltage-time relationships and ion transport of the remaining structures (C-L-A, H-C-L and H-A-L) were investigated (Fig. 4d–f). The currents of the C-L-A, H-C-L and H-A-L components gradually decreased with the discharge time. The voltage of the H-C-L component rapidly decreased and then rose, while the voltages of the C-L-A and H-A-L components gradually declined. As previously analyzed, because the water contents of L, A and C gels were 379.37%, 147.46% and 167.83% respectively, the water of the L gel spread towards A and C gels respectively in the C-L-A component, and the ionization of $ZnCl_2$ near A and C gels was accelerated during this process. Therefore, with the free diffusion of ions, the current and voltage of the C-L-A component gradually decreased with the discharge time. The performances in voltage were different between the H-C-L and H-A-L components, it may be due to the higher water content of C gel (167.83%) than that of A gel

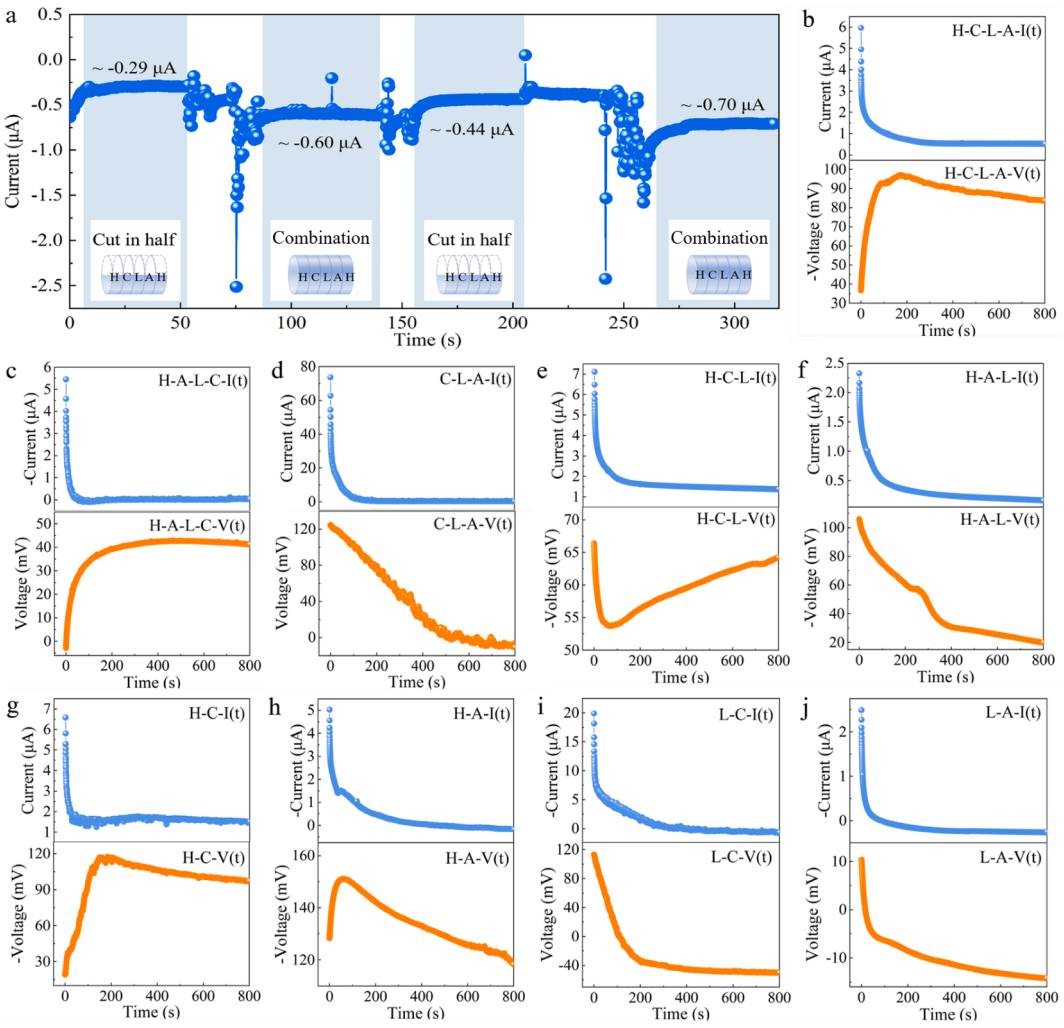

Fig. 4. The combinable abilities of the -H-C-L-A-H device. (a) The current-time relationships of -H-C-L-A-H devices when they were cut in half and reassembled. The current-voltage-time relationships of (b) -H-C-L-A and (c) -H-A-L-C components. The current-voltage-time relationships of (d) C-L-A, (e) -H-C-L and (f) H-A-L components. The current-voltage-time relationships of (g) -H-C, (h) H-A, (i) L-C and (j) L-A components. The instrument collected data every 0.15 s. The minus (-) in front of the currents and voltages in the ordinate titles represented the direction.

(147.46%), which may accelerate the ionization near C gel during this process.

Furthermore, three gels of the H-C-L-A-H device were removed, then the current-voltage-time relationships and ion transport of the remaining parts (H-C, H-A, L-C and L-A) were revealed (Fig. 4g–j). The H-C, H-A, L-C and L-A components were all made by a gel containing $ZnCl_2$ electrolyte and an ion-selective gel, therefore it took on similarity in the behaviors of the currents and voltages. Generally, the currents of the four components declined with discharge time due to the free diffusion of ions in gels. The voltage of the H-C and H-A components increased and then decreased, while the voltage of the L-C and L-A components gradually declined. The reason was that the more Zn^{2+} ions from $ZnCl_2$ ionization in the H gel were involved in a chemical reaction forming the $Zn(OH)_2$ precipitation ($Zn^{2+} + 2OH^- \Leftrightarrow Zn(OH)_2\downarrow$) due to the much higher concentration of $ZnCl_2$ in H gel (1.15 M) than that in L gel (0.0075 M).

The above results indicate that the systemic combinable ability and the structural combinable ability of the H-C-L-A-H device can ensure that the H-C-L-A-H device can continue to operate in case of damage without self-repair, and the undamaged part can work during the reconstruction.

Besides, the H-C-L-A-H device has excellent capabilities of responding to the twisting, bending and folding, and recognizing the external environment either in a rapid or slow collision by the electrical signals, consequently realizing the programmable intelligent identification under the condition of general collision. As shown in Fig. 5a, when the H-C-L-A-H device was attached to the hand, the current showed obvious regular peaks and troughs with the bending and straightening of the hand. This result implied that the H-C-L-A-H device can establish a better information interaction relationship with the body. As illustrated in Fig. 5b, the H-C-L-A-H devices were folded to 30°, 60° and 90° respectively and then restored to 60°, 30° and 0°, where each folding angle was kept for 30 s. The results suggested that there is a corresponding relationship between the change of current and the folding angle. And the currents showed regular changes for continuous twisting whose angle was less than 20°, as revealed in Fig. 5c. The results indicated that the H-C-L-A-H device could establish some information interaction relationships with the body or their surroundings to reflect and identify certain changes. Additionally, the results of Fig. 5d and e indicated that the H-C-L-A-H device can identify the external environment either in a rapid or slow collision by the electrical signals, consequently realizing the programmable intelligent identification under the condition of general collision, which was investigated in the *Supporting Information* (Fig. S3). Also, the results of Fig. 5f suggested that the H-C-L-A-H device could work under high temperatures hardly affected by heat, and this thermal stability was further conducive to the application in

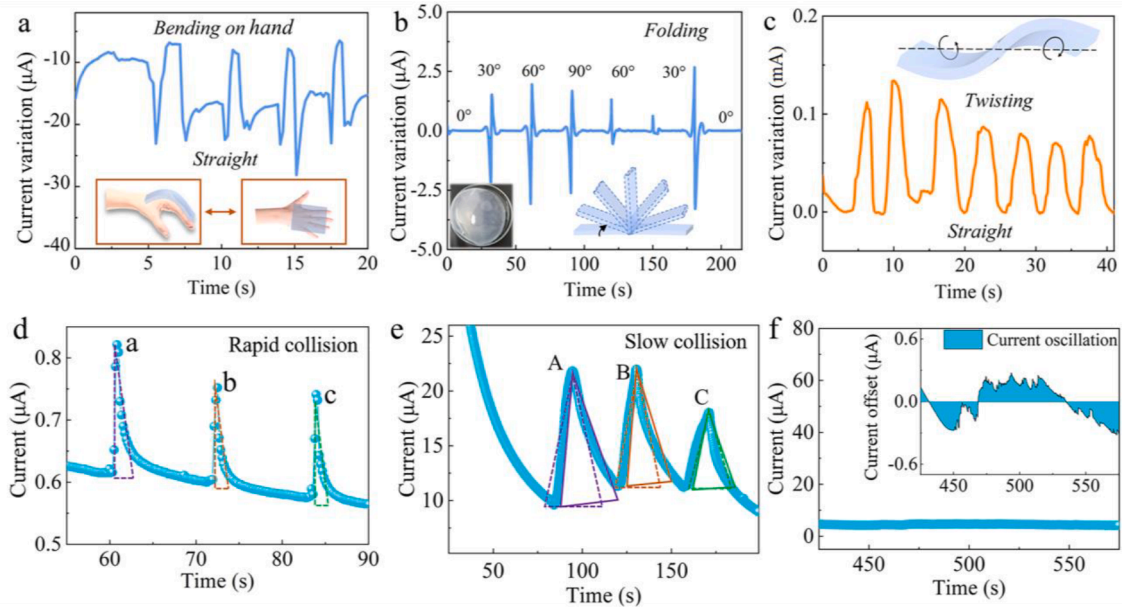

Fig. 5. Responses to bending (a), folding (b), twisting (c), rapid collision (d), slow collision (e) and heat producer (f) of the -H-C-L-A-H device. The folding angles are 0°, 30°, 60°, 90°, 60°, 30° and 0° respectively. And the illustration is the sample used in the actual test. The thickness of each gel round piece was 2 mm (a-c). During the rapid collision, pressures were applied at points a, b and c respectively, and the right-angled triangle models are used to represent relationships between pressure and current variation (d). During the slow collision, pressures were applied at points A, B and C respectively, and the isosceles triangle models are used to describe relationships between pressure and current variation (e). A heat producer is a hot-water bag and the illustration is the current-oscillation relationship (f).

high-temperature conditions (detailed in Fig. S3). The above results prove that the H-C-L-A-H device has application potentials in feedback systems, power transformers, artificial intelligence systems, soft robotics, wearable devices, implanted electronics with flexible characteristics matching biological tissues, etc.

As an application to monitor practical activities in real time, the H-C-L-A-H device was connected to a Bluetooth audio and human throat, responding to various music rhythms and human speaking. Fig. 6 recorded the corresponding resistance response when the H-C-L-A-H device was integrated into a Bluetooth audio and human throat. When the H-C-L-A-H device was connected to the Bluetooth audio, it can be observed that the output signals showed different waveforms with the vibrations of different music rhythms including strong music, slow music and moderate music, as revealed in Fig. 6a and c. There was difference upon different music rhythms and the intensity of strong music was larger than that of slow music and moderate music, while the frequency of slow music will decrease, thus causing different resistance changes during the music vibrations. Strong music had the most significant change in resistance, slow music the least, and moderate music had something in between. Therefore, the results showed that the H-C-L-A-H device was capable of recognizing music information.

In addition, through monitoring the relative change of the resistance of the H-C-L-A-H device, human speaking movements of the throat were further tracked with good repeatability and stability (Fig. 6b and d).

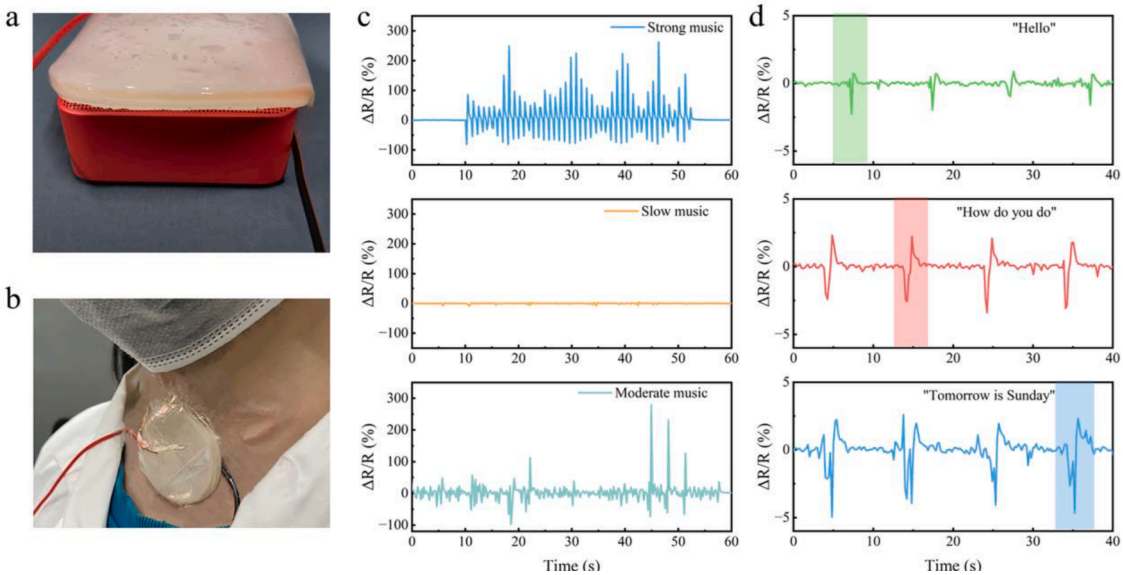

Fig. 6. Responses of the -H-C-L-A-H device to various music rhythms and human speaking. The photo of the actual test in responses to various music rhythms (a) and human speaking (b). The relative change of the resistance with the vibrations of different music rhythms (c) and human speaking movements of the throat (d). Each gel round piece was 2 mm thickness and 10 cm diameter (a-d).

When the H-C-L-A-H device was attached to the throat, it showed stable and unique waveforms with a volunteer speaking the sentences "Hello", "How do you do" and "Tomorrow is Sunday". The waveforms of the resistance changes upon speaking long sentences were more complex than those upon speaking short sentences. This was attributed to the fact that when human was speaking, the vocal cord was vibrating, and the vibrations of vocal cord were more complex with speaking long sentences, outputting the more complex resistance change waveform due to the sensitivity of the H-C-L-A-H device to vibrations. The above results indicate that the H-C-L-A-H device can detect human movements and recognize complex external stimuli, and has further application potentials in feedback systems, artificial intelligence systems, soft robotics, wearable devices, next-generation artificial electric organs, etc.

3. Conclusions

In summary, we designed a flexible and combinable low-power device by imitating the generation of nerve signals whose components can be disassembled. The morphologies, structures and flexible abilities of the H-C-L-A-H device were investigated. Also, the current-voltage-time relationships and ion transport mechanism were revealed, and the effects of the number of cation-selective groups and anion-selective groups on the electrical properties were evaluated respectively. Moreover, the systemic combinable ability and the structural combinable ability of the H-C-L-A-H device were discussed respectively. The results indicate that the H-C-L-A-H device can continue to operate in case of damage without self-repair, and the undamaged part can work during the reconstruction. Additionally, the H-C-L-A-H device exhibits excellent capabilities of responding to twisting, bending and folding, and recognizing the external environment either in a rapid or slow collision by the electrical signals, consequently realizing the programmable intelligent identification under the condition of general collision. Furthermore, the H-C-L-A-H device can be employed to recognize music information and monitor human speaking movements. These advantages make the H-C-L-A-H device provide a meaningful approach for feedback systems, power transformers, artificial intelligence systems, soft robotics, wearable devices, implanted electronics with flexible characteristics matching biological tissues, etc.

4. Methods

4.1. Synthesis of materials

Raw materials comprise acrylamide (Am), N, N'-methylenebisacrylamide (Bis), ammonium persulfate (APS), N, N, N', N'-tetraethylethylenediamine (TEMED), (3-acrylamidopropyl) trimethylammonium chloride solution (75 wt% in H_2O), sodium isethionate, zinc chloride and deionized water. All reagents were purchased from Aladdin Chemical Co., Ltd. The compositions of each gel prepared by the free polymerization method were as follows: L gel: 2.8 M Am, 0.0025 M Bis, 0.0008 M APS, 0.0094 M TEMED, 0.0075 M zinc chloride. H gel: 2.8 M Am, 0.0025 M Bis, 0.0008 M APS, 0.0094 M TEMED, 1.15 M zinc chloride. C gel: 2.8 M Am, 0.0025 M Bis, 0.0008 M APS, 0.0094 M TEMED, 1.2 M sodium isethionate. A gel: 2.8 M Am, 0.0025 M Bis, 0.0008 M APS, 0.0094 M TEMED, 1.2 M (3-acrylamidopropyl) trimethylammonium chloride solution. The raw materials were dispersed in deionized water, and then the mixture was injected into a mold with many holes with 10 mm inner diameter and 5 mm depth. The H, C, L and A gel round pieces with 2 mm thickness and 10 cm diameter were prepared via a mold with 2 mm depth and 10 cm inner diameter to investigate the abilities of twisting, bending and folding. The gels can be obtained by the free radical polymerization. Additionally, the water contents of H, L, A and C gels were 176.05%, 379.37%, 147.46% and 167.83%, respectively.

4.2. Components and morphology characterization

The morphologies of the samples were obtained by scanning electron microscopy (SEM) at 5.0 kV. Fourier transform-infrared spectroscopy (FT-IR) was recorded by a Nicolet 6700 (Thermo Fisher, USA) in the frequency ranges of 400–4000 cm^{-1}.

4.3. Electrical signals, elasticities and hardness characterization

The current-voltage-time relationships of H-C-L-A-H hydrogel components were measured by the Keithley 2400 SourceMeter. The elasticities of C gel, A gel, H gel and L gel were characterized by the Suce SH-III digital push-60 pull meter. The hardness of C gel, A gel, H gel and L gel were investigated by the Nscing LX-A Shore durometer.

The electrochemical impedance spectroscopy (EIS) was obtained by an electrochemical workstation (CHI660E) at room temperature. The ionic conductivity was calculated as following: $\sigma = \frac{L}{R_b \cdot S}$, where σ was the ionic conductivity of the sample and L, R_b, and S represented the thickness of the sample, bulk resistance of the sample, and electrode contacting area, respectively. In the L, H, C and A gels with 0.5 cm thickness and 1 cm diameter, the thickness (L) of each gel is 0.5 cm, and the bulk resistance (R_b) values of the L, H, C and A gels are 19,119.9, 5463.8, 39,090.0, 3551.9 Ω, respectively (Fig. S4, *Supporting information Part 5*), and the electrode contacting area (S) of each gel is 0.785 cm^{-2}. Thus, the ionic conductivity (σ) values of the L, H, C and A gels at room temperature are 3.33×10^{-5}, 1.17×10^{-4}, 1.63×10^{-5}, 1.79×10^{-4} S/cm, respectively.

Data availability

Data will be made available on request.

CRediT authorship contribution statement

Yuanyuan Chen: Data curation, Writing – original draft. **Hanqing Dai:** Conceptualization, Writing – review & editing. **Zhe Hu:** Software. **Jinxin Wei:** Software. **Wenjie Zhou:** Methodology. **Zhongtao Duan:** Investigation. **Zhongjie Cui:** Investigation. **Wei Wei:** Supervision. **Guoqi Zhang:** Writing – review & editing. **Wanlu Zhang:** Writing – review & editing. **Ruiqian Guo:** Funding acquisition, Writing – review & editing.

Declaration of Competing Interest

The authors declare that they have no known competing financial interests or personal relationships that could have appeared to influence the work reported in this paper.

Data availability

Data will be made available on request.

Acknowledgments

This work was supported by the National Natural Science Foundation of China (Grant No. 62074044), Zhongshan-Fudan Joint Innovation Center and Jihua Laboratory Projects of Guangdong Province (X190111UZ190), Shanghai Post-doctoral Excellence Program (2021016) and Shanghai Rising-Star program (Grant No. 22YF1402000).

Supplementary materials

Supplementary material associated with this article can be found, in

the online version, at doi:10.1016/j.apmt.2023.101836.

References

[1] K. Song, H. Seo, D.Seong, S. Kim, K.J. Yu, Y.C. Kim, J. Kim, S.J. Kwon, H.S. Han, I. Youn, H. Lee, D. Son, Adaptive self-healing electronic epineurium for chronic bidirectional neural interfaces, Nat. Commun. 11 (2020) 4195.

[2] Y.S. Choi, Y.Y. Hsueh, J. Koo, Q. Yang, R. Avila, B. Hu, Z. Xie, G. Lee, Z. Ning, C. Liu, Y. Xu, Y.J. Lee, W. Zhao, J. Fang, Y. Deng, S.M. Lee, A.V. Guardado, I. Stepien, Y. Yan, J.W. Song, C. Haney, Y.S. Oh, W. Liu, H.J. Yoon, A. Banks, M. R. MacEwan, G.A. Ameer, W.Z. Ray, Y. Huang, T. Xie, C.K. Franz, S. Li, J.A. Rogers, Stretchable, dynamic covalent polymers for soft, long-lived bioresorbable electronic stimulators designed to facilitate neuromuscular regeneration, Nat. Commun. 11 (2020) 5990.

[3] G.A. Kendir, W. Liu, G. Wang, M. Sivaprakasam, R. Bashirullah, M.S. Humayun, J. D. Weiland, An optimal design methodology for inductive power link with class-E amplifier, IEEE Trans. Circuits Syst. 52 (2005) 857.

[4] S. Choi, H. Lee, R. Ghaffari, T. Hyeon, D.H. Kim, Recent Advances in Flexible and Stretchable Bio-Electronic Devices Integrated with Nanomaterials, Adv. Mater. 28 (2016) 4203.

[5] Y. Zhou, C. Wan, Y. Yang, H. Yang, S. Wang, Z. Dai, K. Ji, H. Jiang, X. Chen, Y. Long, Highly stretchable, elastic, and ionic conductive hydrogel for artificial soft electronics, Adv. Funct. Mater. 29 (2019) 1806220.

[6] Y.J. Hong, H.Jeong, K.W. Cho, N. Lu, D.H. Kim, Wearable and implantable devices for cardiovascular healthcare: from monitoring to therapy based on flexible and stretchable electronics, Adv. Funct. Mater. 29 (2019) 1808247.

[7] C. He, J. Cheng, Y. Liu, X. Zhang, B. Wang, Thin-walled hollow fibers for flexible high energy density fiber-shaped supercapacitors, Energy Mater 1 (2021) 100010.

[8] D. Xiao, X. Lv, J. Fan, Q. Li, Z. Chen, Zn-based batteries for energy storage, Energy Mater 3 (2023) 300007.

[9] Y. Song, J. Min, W. Gao, Wearable and implantable electronics: moving toward precision therapy, ACS Nano 13 (2019) 12280.

[10] S.K. Kang, R.K.J. Murphy, S.W. Hwang, S.M. Lee, D.V. Harburg, N.A. Krueger, J. Shin, P. Gamble, H. Cheng, S. Yu, Z. Liu, J.G. McCall, M. Stephen, H. Ying, J. Kim, G. Park, R.C. Webb, C.H. Lee, S. Chung, D.S. Wie, A.D. Gujar, B. Vemulapalli, A.H. Kim, K.M. Lee, J. Cheng, Y. Huang, S.H. Lee, P.V. Braun, W. Z. Ray, J.A. Rogers, Bioresorbable silicon electronic sensors for the brain, Nature 530 (2016) 71.

[11] R. Sarpeshkar, C.D. Salthouse, J.J. Sit, M.W. Baker, S.M. Zhak, T.K.T. Lu, L. Turicchia, S. Balster, An ultra-low-power programmable bionic ear processor, IEEE Trans Biomed. Eng. 52 (2005) 711.

[12] M. Zhou, D.H. Kang, J. Kim, J.D. Weiland, Shape morphable hydrogel/elastomer bilayer for implanted retinal electronics, Micromachines 11 (2020) 392.

[13] C.C. Kim, H.H. Lee, K.H. Oh, J.Y. Sun, Highly stretchable, transparent ionic touch panel, Science 353 (2016) 682.

[14] M.S. Sarwar, Y. Dobashi, C. Preston, J.K.M. Wyss, S. Mirabbasi, J.D.W. Madden, Bend, stretch, and touch: locating a finger on an actively deformed transparent sensor array, Sci. Adv. 3 (2017) 1602200.

[15] J.Y. Sun, X. Zhao, W.R.K. Illeperuma, O. Chaudhuri, K.H. Oh, D.J. Mooney, J. J. Vlassak, Z. Suo, Highly stretchable and tough hydrogels, Nature 489 (2012) 133.

[16] J.R. McKee, E.A. Appel, J. Seitsonen, E. Kontturi, O.A. Scherman, O. Ikkala, Healable, stable and stiff hydrogels: combining conflicting properties using dynamic and selective three-component recognition with reinforcing cellulose nanorods, Adv. Funct. Mater. 24 (2014) 2706.

[17] Y. Wang, S. Lee, T. Yokota, H. Wang, Z. Jiang, J. Wang, M. Koizumi, T. Someya, A durable nanomesh on-skin strain gauge for natural skin motion monitoring with minimum mechanical constraints, Sci. Adv. 6 (2020) 7043.

[18] Y. Luo, W. Li, Q. Lin, F. Zhang, K. He, D. Yang, X.J. Loh, X. Chen, A morphable ionic electrode based on thermogel for non-invasive hairy plant electrophysiology, Adv. Mater. 33 (2021) 2007848.

[19] G. Ge, Y.Z. Zhang, W. Zhang, W. Yuan, J.K.E. Demellawi, P. Zhang, E.D. Fabrizio, X. Dong, H.N. Alshareef, $Ti_3C_2T_x$ MXene-activated fast gelation of stretchable and self-Healing hydrogels: a molecular approach, ACS Nano 15 (2021) 2698.

[20] Y. Jian, B. Wu, X. Le, Y. Liang, Y. Zhang, D. Zhang, L. Zhang, W. Lu, J. Zhang, T. Chen, Antifreezing and stretchable organohydrogels as soft actuators, Research 2019 (2019) 2384347.

[21] H. Wei, M. Lei, P. Zhang, J. Leng, Z. Zheng, Y. Yu, Orthogonal photochemistry-assisted printing of 3D tough and stretchable conductive hydrogels, Nat. Commun. 12 (2021) 2082.

[22] J. Wen, J. Tang, H. Ning, N. Hu, Y. Zhu, Y. Gong, C. Xu, Q. Zhao, X. Jiang, X. Hu, L. Lei, D. Wu, T. Huang, Multifunctional ionic skin with sensing, UV-filtering, water-retaining, and anti-freezing capabilities, Adv. Funct. Mater. 31 (2021) 2011176.

[23] C. Zhang, S. Liu, X. Huang, W. Guo, Y. Li, H. Wu, A stretchable dual-mode sensor array for multifunctional robotic electronic skin, Nano Energy 62 (2019) 164.

[24] H. Chen, X. Ren, G. Gao, Skin-inspired gels with toughness, antifreezing, conductivity, and remoldability, ACS Appl. Mater. Inter. 11 (2019) 28336.

[25] X. Pan, Q. Wang, P. He, K. Liu, Y. Ni, L. Chen, X. Ouyang, L. Huang, H. Wang, S. Xu, A bionic tactile plastic hydrogel-based electronic skin constructed by a nerve-like nanonetwork combining stretchable, compliant, and self-healing properties, Chem. Eng. J. 379 (2019) 122271.

[26] H. Dai, Y. Chen, W. Dai, Z. Hu, M. Li, W. Zhang, F. Xie, W. Wei, R. Guo, G. Zhang, Design and mechanism of a self-powered and disintegration–reorganization–regeneration power supply with cold resistance, Adv. Mater. 33 (2021) 2101239.

[27] H. Dai, Y. Chen, W. Dai, Z. Hu, F. Xie, W. Xu, Z. Cui, X. Wei, Z. Chen, B. Yang, W. Zhang, W. Wei, R. Guo, G. Zhang, Investigating the electrochemical performance of smart self-powered bionic skin fragment based on bioelectricity generation, Adv. Mater. Technol. 6 (2021) 2000848.

[28] H.P. Cong, P. Wang, S.H. Yu, Highly elastic and superstretchable graphene oxide/polyacrylamide hydrogels, Small 10 (2014) 448.

[29] M. Hu, X. Gu, Y. Hu, T. Wang, J. Huang, C. Wang, Low chemically cross-linked PAM/C-dot hydrogel with robustness and superstretchability in both as-prepared and swelling equilibrium states, Macromolecules 49 (2016) 3174.